ChemPhysChem

Supporting Information

Phase Diagram for a Lysyl-Phosphatidylglycerol Analogue in Biomimetic Mixed Monolayers with Phosphatidylglycerol: Insights into the Tunable Properties of Bacterial Membranes

Christian Wölk, Hala Youssef, Thomas Guttenberg, Helene Marbach, Gema Vizcay-Barrena, Chen Shen, Gerald Brezesinski, and Richard D. Harvey*

Supporting Information

Experimental Methods

Chemicals and sample preparation

1,2-Dipalmitoyl-sn-glycero-3-phospho-(rac-1-glycerol) sodium salt (DPPG) was supplied by Avanti Polar Lipids (Alabaster, AL, USA) and dipalmitoyl-3-aza-dehydroxy lysyl-phosphatidylglycerol (DP3adLPG) was custom synthesised as described by Rehal *et al*. 2019.[1] Both lipids are used as 1 mM solutions in $CHCl_3$ for the preparation of Langmuir monolayers. DPPG and DP3adLPG were premixed in $CHCl_3$ to obtain the desired mixing ratios. The corresponding solutions were spread onto the air/liquid interface and after solvent evaporation the formed monolayers were laterally compressed to the desired lateral pressures π.

Langmuir Isotherms

Pressure-area isotherms for the lipid monolayers were measured on a home-made computer-interfaced Langmuir film balance at a compression rate of $\leq$10 Å^2·(molecule·min)$^{-1}$. Using the Wilhelmy plate method, the surface pressure was measured with a roughened glass plate with an accuracy of ±0.1 mN·m^{-1}, and the area per molecule with an accuracy of ±0.5 Å^2. A connected thermostat was kept at (20 ± 0.1) °C. Lipid solutions in chloroform, at a concentration of 1 mM, were spread carefully from a micro-syringe (Hamilton, Switzerland) onto the aqueous subphases. Before compression, 10 min were given for the evaporation of the organic solvent. All isotherms were measured at least twice for reproducibility.

Infrared reflection-absorption spectroscopy (IRRAS)

The experiments were performed using a Vertex 70 FTIR spectrometer equipped with a liquid nitrogen cooled mercury cadmium telluride detector attached to an external air/water reflection unit (XA-511, Bruker). The principle of the method and its application to Langmuir films at the air/water interfaces has been previously described. A small reference trough and the larger sample trough are alternatively moved into the IR beam path by a shuttle system. The reflectance absorbance was calculated using $-\log(R/R_0)$, with R being the reflectance of the sample and R_0, the reflectance of the reference. The resolution and scanner speed in all experiments were 8 cm^{-1} and 20 kHz. The incident IR beam is polarized with a KRS-5 wire grid polarizer. Spectra are co-added over 200 scans for s-polarized light and over 400 scans for p-polarized light before being apodized using Blackman-Harris 3-term function and fast Fourier transformed after one level of zero filling.[2–7]

Epifluorescence Microscopy

Fluorescence microscopy imaging of monolayers at the air/water interface was performed using an Axio Scope A1 Vario epifluorescence microscope (Carl Zeiss MicroImaging, Jena, Germany) installed above a Langmuir Teflon trough with a maximal area of 264 cm^2 and two moveable computer-controlled Teflon barriers (Riegler & Kirstein, Potsdam, Germany). The trough was positioned on an *x–y* stage (Märzhäuser, Wetzlar, Germany) to be able to move the film surface with respect to the objective lens to any desired position. The *x–y–z* motion control was managed by a MAC5000 system (Ludl Electronic Products, Hawthorne, NY, USA). The trough was housed by a home-built Plexiglas hood to ensure a dust-free environment and to minimize evaporation of water. The temperature of (20.0 ± 0.1) °C was maintained with a circulating water bath, and the whole setup was placed on a vibration-damped optical table (Newport, Darmstadt, Germany). The air/water interface was illuminated using the following setup from Carl Zeiss MicroImaging (Jena, Germany): a 100 W mercury arc lamp (HXP 120 C), a long working distance objective (LD EC Epiplan-

NEOFLUAR 50×), and a filter/beam splitter combination (Filter Set 81HE), to select appropriate wavelengths for the excitation and detection of BODIPY 558/568 C12. Images were recorded using an EMCCD camera (ImageEM C9100-13, Hamamatsu, Herrsching, Germany). Image analysis and data acquisition were done using the AxioVision software (Carl Zeiss MicroImaging, Jena, Germany). All the images acquired were individually contrast-adjusted from the raw data. Lipid solutions with a concentration of 1 mM lipid in chloroform containing only 0.1 mol% fluorescently labelled BODIPY 558/568 C12 were prepared separately. The monolayer was compressed using a compression speed of 2 $Å^2 \cdot molecule^{-1} \cdot min^{-1}$. The microscopy images were taken during the compression of the monolayer.

Grazing incidence X-ray diffraction (GIXD)

The GIXD experiments were performed at the high-resolution diffraction beamline P08 (PETRA III, DESY, Hamburg, Germany)[8] at an incident energy of 15keV (wavelength λ=0.827 Å) at an incident angle 0.07º (85% of the critical angle of water). For the measurements, a Langmuir trough was located in a hermetically sealed container with Kapton windows transparent for X-rays. The trough was constantly flushed with helium (He) to reduce the air scattering background. Approximately 1 mm x 70 mm of the monolayer surface were illuminated. In order to reduce mechanically excited surface waves, a glass block was present in the subphase beneath the illuminated area of the monolayer. A Mythen2 detector (DECTRIS, Baden, Switzerland) was rotated around the sample to detect the intensity of the diffracted beam as a function of the vertical scattering angle α_f and horizontal scattering angle 2θ. A Soller collimator (JJ X-RAY, Denmark) was located between the sample and the detector to restrict the in-plane divergence of the diffracted beam to 0.08º (FWHM). Model peaks taken as Lorentzian in the in-plane (Bragg peaks, Q_{xy}) and Gaussian in the out-of-plane direction (Bragg rods, Q_z) were fitted to the integrated data. Subsequently, the Bragg peak positions respectively the centres of the Bragg rods are obtained and structure relevant information is gained.[9–13]

Total reflection x-ray fluorescence (TRXF)

During recent years, TRXF was established as an element-specific complementary scattering technique.[14–16] The TRXF measurements were carried out at beamline P08 (PETRA III, DESY, Hamburg, Germany) using the above described set-up. The fluorescence signal was detected by an Amptek X-123SDD detector (Amptek, Bedford, USA) placed almost parallel to the liquid surface and perpendicular to the photon beam axis. This detector position was chosen in order to keep the Compton scattering at the given polarization of the photons as low as possible. The footprint centre of the incident beam was adjusted to the middle of the trough length along the beam direction, and at the middle of the view angle of the fluorescence detector.[17,18]

Transmission electron microscopy (TEM)

Cells of a clinically-isolated *Staphylococcus aureus* EMRSA-16 strain were cultured in 200 ml of Brain Heart Infusion (BHI) broth at 37°C for 24 h in a shaking incubator at 115 rpm. After incubation, the culture was centrifuged for 8 minutes at 3,750 rpm in order to obtain a cell pellet, which was washed and centrifuged twice at 8,000 rpm for 8 minutes. The cell pellet was finally re-suspended in 1.5 ml of 2.5% glutaraldehyde in 0.15 M cacodylate buffer (pH 7.3) and stored overnight at 4°C. The cells were then fixed in 1% w/v osmium tetroxide in 0.15 M cacodylate buffer (pH 7.3) for 1 h prior to dehydration through a grade series of ethanol concentrations, and equilibration with propylene oxide. Finally the sample was infused with epoxy embedding resin (TAAB Laboratories Equipment Ltd., UK) and polymerised at 70 °C for 24 h. Ultrathin sections (50-70 nm) were prepared using a

microtome before being mounted onto 150 mesh copper grids and contrasted using uranyl acetate and lead acetate. The sections were examined using an FEI Tecnai 12 transmission electron microscope (Field Emission Inc., USA) operated at 120 kV, with the images acquired with an AMT 16000M camera (Advanced Microscopy Techniques Corp., USA).

Supplementary Results

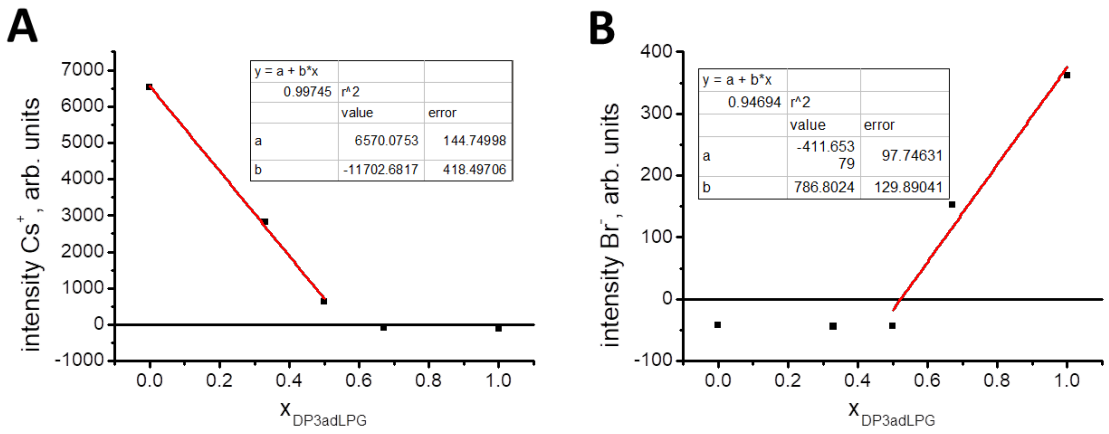

Fig. S1. A) Linear fit of the decreasing Cs intensity versus $x_{DP3adLPG}$. The intersection with the X-axis is at $x_{DP3adLPG} = 0.561$. B) Linear fit of the decreasing Br intensity versus $x_{DP3adLPG}$. The intersection with the X-axis is at $x_{DP3adLPG} = 0.524$.

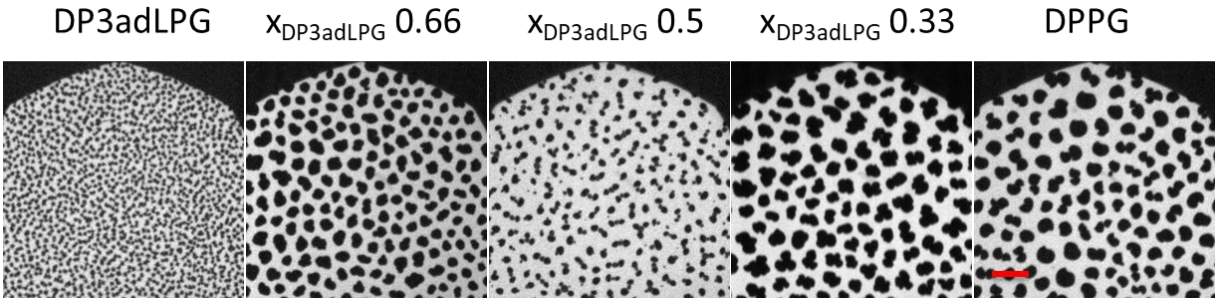

Fig. S2. Representative epifluorescence micrographs of the monolayers at different $x_{DP3adLPG}$ values (indicated) taken in the LE/LC transition region of the isotherms. The scale bar represents 20 µm.

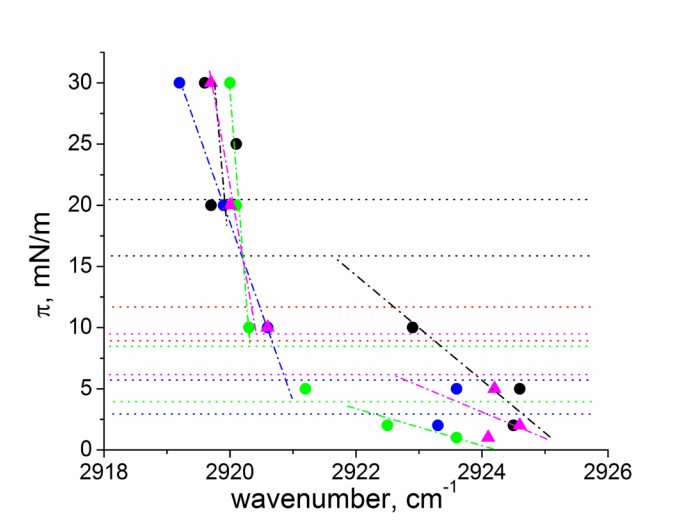

Fig. S3. Wavenumbers of the asymmetric CH_2 stretching vibration taken at different lateral pressures along the isotherms of DP3adLPG (black) and the DPPG/DP3adLPG mixtures 2:1 (blue), 1:1 (green) and 1:2 (magenta) on a pH 7.4 subphase containing 1 mM CsBr at 20 °C. The corresponding plateau region, observed in the isotherms, is indicated (dotted lines). The high wavenumbers in the LE phase indicate a high amount of gauche-conformers. The chains are in all-trans state in the LC phases (wavenumber of 2920 cm^{-1} or below).

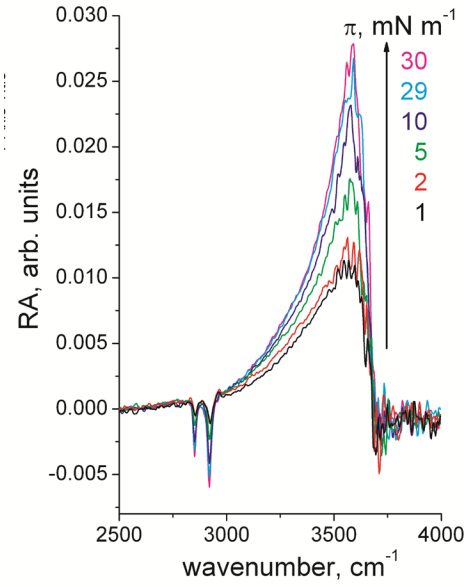

Fig. S4. Part of the IRRA spectra of the DPPG/DP3adLPG 1:1 mixed monolayer on pH 7.4 subphase at 20 °C taken along the isotherm at π = 1, 2, 5, 10, 20, and 30 $mN \cdot m^{-1}$. The spectra are recorded using p-polarized light and an angle of incidence of 40°. The LE-LC phase transition can be seen in the shift of the CH_2 band positions (S3) and in the intensity of the OH-band. The increase in OH-band intensity indicates an increase in the effective thickness/density of the monolayer.

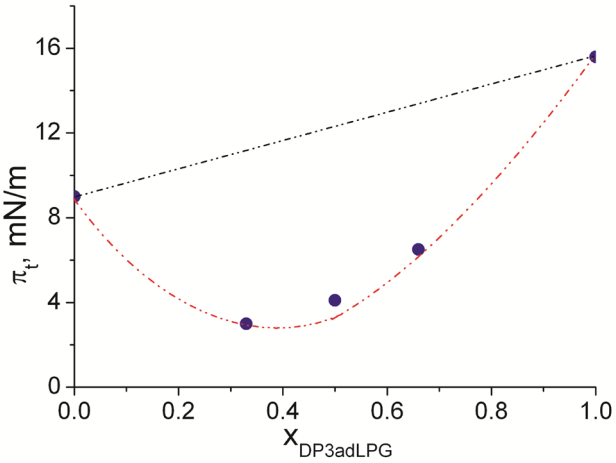

Fig. S5. Transition pressure π_t between LE (liquid-expanded) and LC (condensed) phases of DP3adLPG, DPPG and the corresponding DPPG/DP3adLPG mixtures on a pH 7.4 subphase containing 1 mM CsBr at 20 °C versus the mole fraction $x_{DP3adLPG}$.

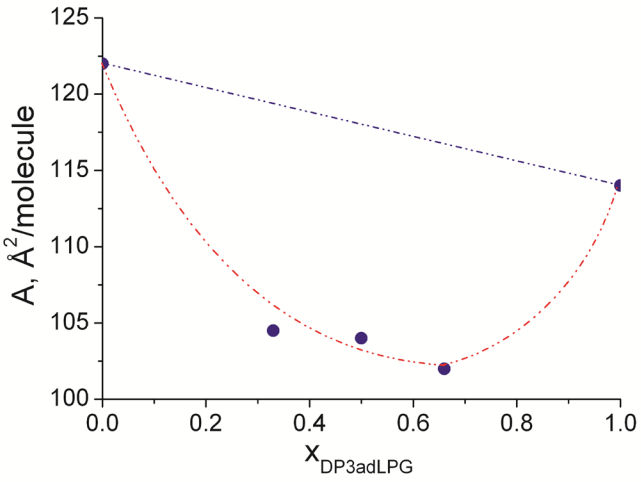

Fig. S6. The molecular area, taken from the isotherms (Fig. 1) at 2 mN·m^{-1}, versus the mole fraction $x_{DP3adLPG}$.

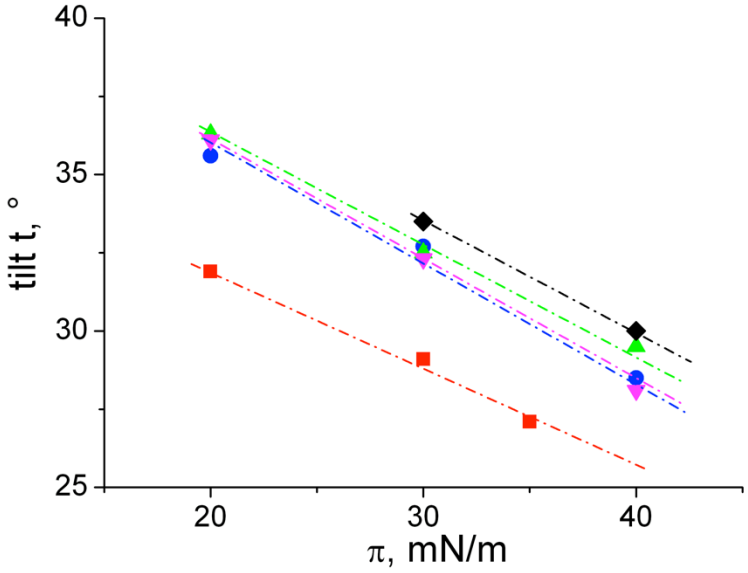

Fig. S7. Tilt angle t of DPPG (■), DP3adLPG (♦) and the DPPG/DP3adLPG mixtures 2:1 (blue ●), 1:1 (green ▲) and 1:2 (magenta ▼) on a pH 7.4 subphase containing 1 mM CsBr at 20 °C versus the lateral pressure π.

Table S1. GIXD results of monolayers of ***DPPG*** on pH 7.4 at 20 °C and different surface pressures: (A) Bragg peak (Q_{xy}) and Bragg rod (Q_z) positions and the corresponding full-widths at half-maximum. (B) Lattice parameters a, b, c, α, β, γ, lattice distortion d, tilt angle t, chain in-plane area A_{xy}, chain cross-sectional area A_0.

(A)

Π, mN/m	$Q_{xy}(1)$, Å^{-1}	$Q_z(1)$, Å^{-1}	$Q_{xy}(2)$, Å^{-1}	$Q_z(2)$, Å^{-1}	$Q_{xy}(3)$, Å^{-1}	$Q_z(3)$, Å^{-1}
20	1.352 0.066	0.769 0.30	1.394 0.075	0.657 0.30	1.473 0.020	0.112 0.30
30	1.377 0.042	0.699 0.30	1.406 0.044	0.602 0.30	1.479 0.016	0.097 0.30
35	1.399 0.060	0.663 0.30	1.428 0.058	0.549 0.30	1.485 0.019	0.114 0.30

(B)

Π, mN/m	a/b/c, Å	α/β/γ, °	d	t, °	A_{xy}, Å^2	A_0, Å^2
20	4.979 5.134 5.425	123.8 121.1 115.1	0.10140	31.9	23.1	19.6
30	4.964 5.068 5.331	123.0 121.1 115.8	0.08597	29.1	22.6	19.8
35	4.922 5.024 5.225	122.6 120.7 116.6	0.07058	27.1	22.1	19.7

Table S2. GIXD results of monolayers of ***DPPG/DP3adLPG 2/1*** on pH 7.4 at 20 °C and different surface pressures: (A) Bragg peak (Q_{xy}) and Bragg rod (Q_z) positions and the corresponding full-widths at half-maximum. (B) Lattice parameters a, b, c, α, β, γ, lattice distortion d, tilt angle t, chain in-plane area A_{xy}, chain cross-sectional area A_0.

(A)

Π, mN/m	$Q_{xy}(1)$, Å^{-1}	$Q_z(1)$, Å^{-1}	$Q_{xy}(2)$, Å^{-1}	$Q_z(2)$, Å^{-1}	$Q_{xy}(3)$, Å^{-1}	$Q_z(3)$, Å^{-1}
20	1.325 0.055	0.790 0.30	1.467 0.016	0 0.30		
30	1.361 0.056	0.735 0.32	1.473 0.018	0 0.32		
40	1.394 0.087	0.642 0.31	1.478 0.022	0 0.31		

(B)

Π, mN/m	a/b/c, Å	α/β/γ, °	d	t, °	A_{xy}, Å^2	A_0, Å^2
20	5.694 5.143 5.143	112.8 123.6 123.6	0.14001	35.6	24.4	19.8
30	5.490 5.072 5.072	114.5 122.8 122.8	0.10807	32.7	23.4	19.7
40	5.316 5.014 5.014	116.0 122.0 122.0	0.07948	28.5	22.6	19.9

Table S3. GIXD results of monolayers of ***DPPG/DP3adLPG 1/1*** on pH 7.4 at 20 °C and different surface pressures: (A) Bragg peak (Q_{xy}) and Bragg rod (Q_z) positions and the corresponding full-widths at half-maximum. (B) Lattice parameters a, b, c, α, β, γ, lattice distortion d, tilt angle t, chain in-plane area A_{xy}, chain cross-sectional area A_0.

(A)

Π, mN/m	$Q_{xy}(1)$, Å^{-1}	$Q_z(1)$, Å^{-1}	$Q_{xy}(2)$, Å^{-1}	$Q_z(2)$, Å^{-1}	$Q_{xy}(3)$, Å^{-1}	$Q_z(3)$, Å^{-1}
20	1.314 0.027	0.849 0.30	1.330 0.039	0.762 0.30	1.466 0.015	0.087 0.30
30	1.346 0.025	0.768 0.30	1.364 0.043	0.669 0.30	1.472 0.016	0.099 0.30
40	1.378 0.034	0.699 0.30	1.388 0.060	0.618 0.30	1.477 0.017	0.081 0.30

(B)

Π, mN/m	a/b/c, Å	α/β/γ, °	d	t, °	A_{xy}, Å^2	A_0, Å^2
20	5.119 5.182 5.711	124.2 123.1 112.7	0.14282	36.3	24.5	19.7
30	5.050 5.118 5.523	123.5 122.3 114.2	0.11419	32.5	23.6	19.9
40	5.013 5.050 5.373	122.6 121.9 115.4	0.08986	29.5	22.9	19.9

Table S4. GIXD results of monolayers of ***DPPG/DP3adLPG 1/2*** on pH 7.4 at 20 °C and different surface pressures: (A) Bragg peak (Q_{xy}) and Bragg rod (Q_z) positions and the corresponding full-widths at half-maximum. (B) Lattice parameters a, b, c, α, β, γ, lattice distortion d, tilt angle t, chain in-plane area A_{xy}, chain cross-sectional area A_0.

(A)

Π, mN/m	$Q_{xy}(1)$, Å^{-1}	$Q_z(1)$, Å^{-1}	$Q_{xy}(2)$, Å^{-1}	$Q_z(2)$, Å^{-1}	$Q_{xy}(3)$, Å^{-1}	$Q_z(3)$, Å^{-1}
20	1.321 0.033	0.845 0.30	1.330 0.062	0.762 0.30	1.466 0.016	0.083 0.30
30	1.352 0.037	0.770 0.31	1.370 0.098	0.663 0.31	1.471 0.016	0.107 0.31
40	1.378 0.040	0.682 0.30	1.425 0.069	0.567 0.30	1.476 0.018	0.115 0.30

(B)

Π, mN/m	a/b/c, Å	α/β/γ, °	d	t, °	A_{xy}, Å^2	A_0, Å^2
20	5.127 5.162 5.689	123.9 123.3 112.8	0.13870	36.1	24.4	19.7
30	5.043 5.110 5.487	123.3 122.1 114.6	0.10712	32.3	23.4	19.8
40	4.926 5.094 5.276	123.3 120.2 116.5	0.07936	28.1	22.5	19.8

Table S5. GIXD results of monolayers of ***DP3adLPG*** on pH 7.4 at 20 °C and different surface pressures: (A) Bragg peak (Q_{xy}) and Bragg rod (Q_z) positions and the corresponding full-widths at half-maximum. (B) Lattice parameters a, b, c, α, β, γ, lattice distortion d, tilt angle t, chain in-plane area A_{xy}, chain cross-sectional area A_0.

(A)

Π, mN/m	$Q_{xy}(1)$, Å^{-1}	$Q_z(1)$, Å^{-1}	$Q_{xy}(2)$, Å^{-1}	$Q_z(2)$, Å^{-1}	$Q_{xy}(3)$, Å^{-1}	$Q_z(3)$, Å^{-1}
20						
30	1.328 0.038	0.790 0.31	1.351 0.042	0.678 0.31	1.470 0.017	0.112 0.31
40	1-351 0.049	0.730 0.31	1.387 0.054	0.577 0.31	1.471 0.029	0.153 0.31

(B)

Π, mN/m	a/b/c, Å	α/β/γ, °	d	t, °	A_{xy}, Å^2	A_0, Å^2
20						
30	5.069 5.157 5.611	124.0 122.5 113.4	0.12883	33.5	24.0	20.0
40	4.999 5.132 5.443	123.7 121.3 115.0	0.10204	30.0	23.2	20.1

References

[1] R. Rehal, P. R. J. Gaffney, A. T. M. Hubbard, R. D. Barker, R. D. Harvey, *Eur. J. Pharm. Sci.* **2019**, *128*, 43–53.

[2] C. R. Flach, A. Gericke, R. Mendelsohn, *J. Phys. Chem. B* **1997**, *101*, 58–65.

[3] R. A. Dluhy, R. Mendelsohn, H. L. Casal, H. H. Mantsch, *Biochemistry* **1983**, *22*, 1170–1177.

[4] R. Mendelsohn, G. Mao, C. R. Flach, *Biochim. Biophys. Acta - Biomembr.* **2010**, *1798*, 788–800.

[5] R. Mendelsohn, *Annu. Rev. Phys. Chem.* **1995**, *46*, 305–334.

[6] R. Mendelsohn, C. R. Flach, *Curr. Top. Membr.* **2002**, *52*, 57–88.

[7] A. H. Muenter, J. Hentschel, H. G. Borner, G. Brezesinski, *Langmuir* **2008**, *24*, 3306–3316.

[8] O. H. Seeck, C. Deiter, K. Pflaum, F. Bertam, A. Beerlink, H. Franz, J. Horbach, H. Schulte-Schrepping, B. M. Murphy, M. Greve, et al., *J. Synchrotron Radiat.* **2012**, *19*, 30–38.

[9] J. Als-Nielsen, D. Jacquemain, K. Kjaer, F. Leveiller, M. Lahav, L. Leiserowitz, *Phys. Rep.* **1994**, *246*, 251–313.

[10] D. Jacquemain, S. G. Wolf, F. Leveiller, M. Deutsch, K. Kjaer, J. Als-Nielsen, M. Lahav, L. Leiserowitz, *Angew. Chemie Int. Ed. English* **1992**, *31*, 130–152.

[11] V. M. Kaganer, H. Möhwald, P. Dutta, *Rev. Mod. Phys.* **1999**, *71*, 779–819.

[12] K. Kjaer, *Phys. B Phys. Condens. Matter* **1994**, *198*, 100–109.

[13] C. Stefaniu, G. Brezesinski, *Curr. Opin. Colloid Interface Sci.* **2014**, *19*, 216–227.

[14] W. Bu, D. Vaknin, *J. Appl. Phys.* **2009**, *105*, 084911.

[15] J. Daillant, L. Bosio, J. J. Benattar, C. Blot, *Langmuir* **1991**, *7*, 611–614.

[16] V. L. Shapovalov, M. E. Ryskin, O. V. Konovalov, A. Hermelink, G. Brezesinski, *J.*

Phys. Chem. B **2007**, *111*, 3927–3934.
[17] C. Stefaniu, V. M. Latza, O. Gutowski, P. Fontaine, G. Brezesinski, E. Schneck, *J. Phys. Chem. Lett.* **2019**, *10*, 1684–1690.
[18] G. Brezesinski, E. Schneck, *Langmuir* **2019**, *35*, 8531–8542.